University of Wollongong

Research Online

Faculty of Science, Medicine and Health - Papers: Part B

Faculty of Science, Medicine and Health

1-1-2019

Luminescence chronology of the Palaeolithic-Neolithic transition in the Yujiagou site at the Nihewan Basin, northern China

Xue Rui
University of Wollongong, xr145@uowmail.edu.au

Yujie Guo
Peking University, yg991@uowmail.edu.au

Jia-Fu Zhang
Peking University

Yue Hu
University of Wollongong, yh280@uowmail.edu.au

Hui Mei
Hebei Normal University

See next page for additional authors

Follow this and additional works at: https://ro.uow.edu.au/smhpapers1

Publication Details Citation

Rui, X., Guo, Y., Zhang, J., Hu, Y., Mei, H., Wang, Y., Xie, F., & Li, B. (2019). Luminescence chronology of the Palaeolithic-Neolithic transition in the Yujiagou site at the Nihewan Basin, northern China. Faculty of Science, Medicine and Health - Papers: Part B. Retrieved from https://ro.uow.edu.au/smhpapers1/578

Research Online is the open access institutional repository for the University of Wollongong. For further information contact the UOW Library: research-pubs@uow.edu.au

Luminescence chronology of the Palaeolithic-Neolithic transition in the Yujiagou site at the Nihewan Basin, northern China

Abstract

The relationship between the Palaeolithic-Neolithic cultural transition and environmental changes is important for understanding human history. However, the timing and nature of human behaviour at the transition, and their relationship to local environmental conditions, remain poorly understood. The Yujiagou archaeological site in the Nihewan Basin, northern China, provides valuable chronological and archaeological information about cultural changes in northern China due to its continuous archaeological sequence of cultural layers from the Palaeolithic to Neolithic. In this study, we apply post-infrared infrared stimulated luminescence (pIRIR) dating on individual feldspar grains to date the Yujiagou deposits. We provide a revised chronology for the archaeological sequence at the site. We combine these results with multi-proxy climatic indicators to gain insights into palaeoenvironmental changes in the region. The results show that the age of the artefact-bearing deposits ranges from 13.5 to 9.7 ka. Polished stones and pottery begin to occur in the archaeological layer around 13 ka, corresponding to a transitional period when the local climate changed from cold to warm. This site provides evidence for understanding the process that led to the regional transition from hunter-gathering to farming.

Publication Details

Rui, X., Guo, Y., Zhang, J., Hu, Y., Mei, H., Wang, Y., Xie, F. & Li, B. (2019). Luminescence chronology of the Palaeolithic-Neolithic transition in the Yujiagou site at the Nihewan Basin, northern China. Journal of Quaternary Science, 34 (2), 125-137.

Authors

Xue Rui, Yujie Guo, Jia-Fu Zhang, Yue Hu, Hui Mei, You-Ping Wang, Fei Xie, and Bo Li

This journal article is available at Research Online: https://ro.uow.edu.au/smhpapers1/578

Luminescence chronology of the Paleolithic-Neolithic transition in the Yujiagou site at the Nihewan Basin, north China

Xue Rui[1], Yu-Jie Guo[2], Jia-Fu Zhang[3], Yue Hu[1], Hui-Jie Mei[2], You-Ping Wang[4], Fei Xie[5], Bo Li[1,6*]

[1] Centre for Archaeological Science, School of Earth and Environmental Science, University of Wollongong, Wollongong, 2522 NSW, Australia
[2] Institute of Nihewan Archaeology, Hebei Normal University, 050024 Shijiazhuang, Hebei Province, China
[3] MOE Laboratory for Earth Surface Process, Department of Geography, College of Urban and Environmental Sciences, Peking University, 100871 Beijing, China
[4] School of Archaeology and Museology, Peking University, 100871 Beijing, China
[5] Cultural Relics of Hebei Province, 050000 Shijiazhuang, China
[6] Australian Research Council (ARC) Centre of Excellence for Australian Biodiversity and Heritage, University of Wollongong, Wollongong, NSW 2522, Australia

Corresponding to: bli@uow.edu.au

Abstract

The relationship between Paleolithic-Neolithic cultural transition and environmental changes is important for understanding human history. However, the timing and nature of human behaviour of the transition, and their relationship to local environmental conditions, remain poorly understood. The Yujiagou archaeological site in the Nihewan Basin, north China, provides valuable chronological and archaeological information about cultural changes in north China due to its continuous archaeological sequence of cultural layers from Paleolithic to Neolithic. In this study, we apply post-infrared infrared stimulated luminescence (pIRIR) dating on individual feldspar grains to date the deposits of Yujiagou. We hereby provide a revised chronology for the archaeological sequence at the site. We combine these results with multi-proxy climatic indicators to gain insights into the paleoenvironmental changes of the region. The results show that the age of the artefact-bearing deposits range from 13.5 to 9.7 ka. The polished stones and potteries started to occur in the archaeological layer around 13 ka, corresponding to a transitional period when the local climate changed from cold to warm. This site provides evidence for understanding the process that led to the regional transition from hunting-foraging to farming.

KEYWORDS: Paleolithic-Neolithic transition, single grain, post-IR IRSL, Holocene, luminescence dating

1 Introduction

The transition from foraging to cultivation and animal husbandry is one of the most major revolutions in the history of humankind, namely the Neolithic revolution. To find out the reasons why some human societies changed their subsistence strategy, research on sites documenting the process of changing from small mobile hunter-gather to larger group of sedentary agriculturalists are necessary. The Yujiagou site, located in the north-eastern of the Nihewan Basin, north China, contains evidence of human occupation spanning from Late Paleolithic to Neolithic (Mei, 2007), providing ideal archaeological and environmental records for understanding the temporal dimension

of changes in human behaviour and its relationship with environmental changes. Further research on Yujiagou site, however, has been hampered by questionable chronology.

The first chronological study for the Yujiagou site was conducted by Chen (1999) using thermoluminescence (TL) on pottery shard, which yielded a single TL age of ~11.6 ka. Based on TL dating on fine-grain quartz from sediments, Xia et al. (2001) provided five TL ages ranging from ~2.1 to ~12.2 ka for the whole section. They also discussed the environmental background of the site based on climatic proxies. However, the TL chronology on sediments may be questionable, because TL signals are hard to be bleached by sunlight and equivalent dose (D_e) measurements using TL may be affected by sensitivity change (Aitken, 1985), both may result in erroneous results. Compared to TL dating, optical dating of sediments has advantages of being able to be fully and quickly reset by sunlight (Huntley et al., 1985; Aitken, 1998), and, furthermore, reliable measurement procedures have been established to overcome sensitivity changes (e.g., Murray and Wintle, 2000; Roberts et al., 2015).

Optical dating is commonly achieved by measuring the optically stimulated luminescence (OSL) from quartz or the infrared stimulated luminescence (IRSL) from feldspars (Aitken, 1998). Based on IRSL dating on fine polymineral grains, Nagatomo et al. (2009) reported two IRSL ages of ~9 ka for the samples from the Yujiagou site, but without any fading correction and stratigraphic information for their samples. Since it has been shown that the low-temperature IRSL signal from feldspars in this region suffers from anomalous fading (Guo et al., 2016), these IRSL ages may be underestimated. In a recent study on single-grain quartz from this site, Rui et al. (2018) found that the quartz OSL signal is thermally unstable and may result in significant age underestimation in age. Without a reliable chronological framework, it is difficult to discuss the environmental background and archaeological implication of this site. To address this problem, here we applied the newly developed post-IR IRSL measurements to overcome the anomalous fading (Thomsen et al., 2008; Li and Li, 2011; Blegen et al., 2015). We measured individual K-feldspar grains to test and identify incomplete signal resetting or post-depositional mixing of sediments (Jacobs and Roberts, 2007; Jacobs et al., 2011). We established a reliable chronological frame for the Yujiagou site. With the revised chronology, we discuss the environment background of the Yujiagou site and its implication to the process of change from small mobile hunter-gather to larger group of sedentary agriculturalists.

2 Stratigraphy and archaeological contexts

The Yujiagou site (114°28’47”E, 40°09’49”N, 865 m a.s.l.) is located at the northeastern edge of the Nihewan Basin (Fig. 1b). This site is situated on the second river terrace of the Yujiagou gully — one of the tributary of the Sanggan River (Xie et al., 2006). The deposits of the site are mainly water-lain and reworked loess material. The Yujiagou site was discovered in 1965 and first excavated in 1972 – 1974 by the Institution of Vertebrate Paleontology and Paleoanthropology, Chinese Academy of Sciences. In 1995 – 1999, the second excavation was conducted by a joint archaeological team of Cultural Relics of Hebei Province and School of Archaeology and Museology, Peking University. This site consists of two trenches (Yujiagou and Yujiagou_A) several meters away from each other, with exposed areas of about 80 and 40 m^2, respectively. The sedimentary profiles of the two trenches are identical and were divided into seven stratigraphic layers, including Layers 1 to 7 from the top to the bottom (Mei, 2007) (Fig. 2), based on the colour and texture of the deposits. The sedimentary features of each layer were described by Mei (2007) and are summarised as follow:

Layer 1: disturbed surface soil (~0.3 m thick). Pottery and ceramic fragments were recovered from this layer.

Layer 2: black-brown clayey silt layer with plant root (~1.3 m thick). A total of 631 remains were excavated from this layer (from both Yujiagou and Yujiagou_A), including 389 knapped stone artefacts, 11 polished stone artefacts, 7 bone tools, 27 pottery shards, 3 ornaments, 8 burned bones, 9 rocks and 177 animal remains. The knapped stone artefacts consist of hard hammers (n = 2), cores (n = 18), microcores (n = 3, two cylindrical and one conical microcores), flakes (n = 201), bipolar flakes (n = 1), microblades (n = 23), blades (n = 3), tools (n = 40), chunks and debris (n = 98). The tool assemblage is composed of single scrapers (n = 11), double scrapers (n = 5), multiple-edge scrapers (n = 1), end scrapers (n = 4), transverse scrapers (n = 2), points (n = 2), borers (n = 1), arrowheads (n = 4), notches (n = 2), denticulate (n = 1), chopper (n = 1), multi-function tools (n = 4) and unidentified tools (n = 2). The polished stone artefacts include one stone shovel, one millstone, three stone rods, three stone axes, one stone arrowhead and two broken fragments of unidentified tools. The bone tools are composed of one bone dagger and six bone awls. One kiln site and one tomb were also recovered from the bottom of this layer.

Layer 3a: dark yellow-brown clayey silt layer with a loose texture (~1.5 m thick): a total of 784 remains were recovered from this layer, including 292 knapped stone artefacts, 1 polished stone artefact (stone axe), 2 pottery shards, 2 ornaments, 18 burned bones, 4 natural gravels and 465 animal remains. Fig. 3a shows the stone axe, which is polished overall with an oval-shaped cross-section. It is 102 mm in length, 16 mm in thickness. The haft part and cutting edge are 15.4 mm and 39 mm in length respectively. There are only 177 of the total knapped stone artefacts being analyzed, consisting of cores (n = 2), bipolar core (n = 1), wedge-shaped microcores (n = 9), conical microcores (n = 2) (e.g. Fig. 3b), flakes (n = 90), retouched flakes (n = 6), spalls (n = 4) (e.g. Fig. 3c), microblades (n = 7), tools (n = 40) and chunks and debris (n = 16). The tool assemblage is composed of single scrapers (n = 14), double scrapers (n = 2), multi-edge scraper (n = 1), end scrapers (n = 5), transverse scrapers (n = 2), notches (n = 5), points (n = 3), arrowhead (n = 1), borer (n = 1), adze (n = 1) and multi-function tools (n = 5).

Layer 3b: light yellow-brown clayey silt layer with a compact texture (~1.3 m thick). A total of 16,127 remains were recovered from this layer, including 3,689 knapped stone artefacts, 1 polished hornwork, 8 pottery shards, 19 ornaments, 534 burned bones, 28 rocks and 11848 animal remains. The numbered and analyzed knapped stone artefacts consist of cores (n = 8), bipolar cores (n = 6), wedge-shaped microcores (n = 86), cylindrical microcore (n = 1), boat-shaped like microcore (n = 1), flakes (n = 573), retouched flakes (n = 43), spalls (n = 22), blades (n = 2), microblades (n = 97), tools (n = 211) and chunks and debris (n = 124). The stone tool assemblage includes choppers (n = 6), scrapers (n = 149), notches (n = 9), denticulate (n = 3), points (n = 8), spearheads (n = 2), arrowheads (n = 1), awls (n = 6), borers (n = 3) and multi-function tools (n = 24). Two stone mills were recovered from this layer.

Layer 4: a grey-yellow clayey silt layer (~0.6 m thick). A total of 11,199 remains were recovered from this layer, including 6,793 knapped stone artefacts, 1 polished stone artefact, 3 pottery shards, 11 ornaments, 630 burned bones, 3 rocks and 3,758 animal remains. One broken stone mill was recovered from the top of this layer, which is made of reddish brown sandstone (Fig. 3d). It is 94 mm in diameter and 8 mm in thickness.

Layer 5: a brown clayey silt layer (~0.8 m thick): stone artefacts were mostly from the lower part of this layer, and a total of 1,315 remains were recovered from this layer, including 408 knapped stone artefacts, two ornaments, 46 burned bones and 859 animal remains. Ochre (red mudstone and hematite) were also recovered.

Layer 6: a grey-green silt layer inter-bedded with brown coarse sands (~0.3 m thick): a total of 517 remains were recovered from this layer, including 107 knapped stone artefacts (wedge-shaped microcores, microblades, scrapers, etc.), 15 burned bones and 395 animal remains.

Layer 7: sand with gravels (> 0.4 m thick): a total of 1,225 remains were recovered from this layer, including 291 knapped stone artefacts (wedge-shaped microcores, end scrapers, spearheads, choppers, etc.), one ornaments, 20 burned bones and 913 animal remains.

The raw materials of the stone artefacts are dominated by quartzite, followed by flint and agate, and then a small number made of other kind of rocks (hornstone, tuff, mudstone, siliceous rock, etc.). As a huge number of microliths were found in Layers 5 – 7 without any polished stone or pottery shard, these layers were considered to be associated with Paleolithic stage (Xia et al., 2001; Mei, 2007). Layers 3a – 4 contain a small number of polished stones and pottery shards, which became abundant in Layer 2. Xia et al. (2001) and Mei (2007) proposed that Layers 3a – 4 represent the transition period from Paleolithic to Neolithic, and Layer 2 is corresponding to Neolithic stage.

3 Samples and methods

A total of 10 sediment samples were collected from Layers 1 to 5 at Yujiagou (Fig. 2, Table 1). We did not take samples from the gravel layer (Layer 7), because we could not find materials suitable for dating. The lowest sample (YJG-10) was collected from the boundary between Layer 5 and 6. All the samples were collected either using stainless steel tubes or as blocks. After the samples were removed from the section, they were immediately sealed with light-proof materials and transported to the Luminescence Dating Laboratory at the University of Wollongong for preparation and analysis.

3.1 Sample preparation

Sample preparation was conducted under subdued red-light conditions. About 2 cm from both ends of the sampling tubes and the outer surface (~1 cm) of the sample blocks were removed, as they may potentially be exposed to sunlight during sampling, and were used for determining environmental dose rates. The interior samples were used to isolate quartz and potassium-rich feldspar (K-feldspar) grains for equivalent dose (D_e) determination. The samples were treated with hydrochloric acid (HCl) and hydrogen peroxide (H_2O_2) to remove carbonates and organic material, respectively. Fractions of grains of 180–212 μm diameter were separated by wet sieving. Density separation using sodium polytungstate solutions were used to isolate quartz and K-feldspar. The quartz and K-feldspar fractions were then etched in 40% and 10% hydrofluoric acid (HF) acid, respectively, for 40 min to remove the alpha-irradiated outer layer and remove any feldspar grains from the quartz fraction. After HF etching, they were rinsed with 10% HCl to remove any fluorides formed during HF etching. Finally, these grains were dried and re-sieved to recover grains in selected size fraction.

3.2 Dose-rate measurements

For the estimation of the environmental dose rate, the U and Th contents were determined by using a Thick Source Alpha Counting (TSAC) technique, and the K concentrations were obtained using X-ray Fluorescence (XRF). Cosmic-ray dose rates were estimated from the burial depth of each sample and the latitude, longitude and altitude of the site (Prescott and Hutton, 1994). As the last excavation was conducted in 1990s, the section had been exposed for nearly two decades before sampling. The sediments were thus partly dried up, so the water contents measured from our sample (ranging from 1.3 to 2.2 %) should not represent their long-term effective water contents. We have used a value of 15 ± 5% for all the samples, recommended by Guo et al. (2016) for their samples from the same region.

For the calculation of the internal dose rate, Phenom XL Scanning Electron Microscope (SEM) analysis was conducted to measure 21 K-feldspar grains from sample YJG-8 that were accepted for D_e determination. For each grain, one or two arbitrary points on the polished surface were measured. The K content ranges from ~11 to ~13% (Table 2), so we have used about a value of 12 ± 1% for internal K content. Minor contribution from Rb was calculated by assuming a concentration of 400 ± 100 ppm (Huntley and Hancock, 2001). The dosimetry data for all samples are summarised in Table 1.

3.3 Single-grain feldspar measurement

We first conducted OSL measurement on quartz grains. However, a large grain-to-grain variation in thermal stability was identified on single-grain quartz from our samples based on pulse-annealing measurement (Rui et al., 2018). The short lifetime of unstable quartz grains resulted in significant underestimation in D_e estimation. We, therefore, dated our samples based on the pIRIR signals from K-feldspar grains. The K-feldspar grains were measured using a Risø OSL/TL reader (DA-20) equipped with automated sample changer, heater plate, infrared diode (875 nm), calibrated $^{90}Sr/^{90}Y$ beta source, and single grain attachment (Bøtter-Jensen et al., 2003). A 150 mW infrared (IR) laser (830 nm) was used for stimulating individual K-feldspar grains. The beam from the IR laser is focused down to ~30 µm across a grid of 10 × 10 holes drilled into the surface of 9.7 mm diameter sample discs (Bøtter-Jensen et al., 2000). The stimulated signal was measured with an Electron Tubes 9235B photo-multiplier (PM) tube through a blue filter pack of Schott BG-39 and Corning 7-59 filters.

D_e measurements were made using the single-grain pIRIR procedure (Table 3) proposed by Blegen et al. (2015). In this procedure, all the grains from the same disc were firstly bleached at 200 °C for 200 s using IR diodes, and then the pIRIR signals from individual grains were stimulated at 275 °C for 1.5 s using IR laser. A high-temperature bleach at 340 °C for 100 s was conducted at the end of each SAR cycle. The dose response curve (DRC) for each grain is constructed using the sensitivity-corrected pIRIR signals (L_x/T_x) induced from a series of regenerative doses, including a duplicate dose and a zero dose to monitor the recycling ratio and the extent of recuperation, respectively. The D_e value of each grain was obtained by interpolating the sensitivity-corrected natural pIRIR signal (L_n/T_n) on to its corresponding DRC, which was fitted using general order kinetic (GOK) function (Guralnik et al., 2015). The data analysis involved in D_e determination was achieved using the R (R Core Team, 2016) and R packages *numOSL* (Peng et al., 2013; Peng and Li, 2017) and *Luminescence* (Kreutzer et al., 2012).

The net pIRIR signals used for D_e estimation were calculated as the sum of counts in the first 0.15 s of pIRIR decay minus a 'late light' background estimated from the mean count rate over the final 0.15 s. Grains were held for 0.05 s before and after IR stimulation to monitor any interference from isothermal decay. Grains were rejected if the resulting pIRIR data failed to satisfy a series of well-established criteria similar to those proposed by Jacobs et al. (2006), namely if: (1) the initial T_n signal is less than 3 sigma above its corresponding background or its relative error is >25%; (2) the recuperation ratio is larger than 5% (the ratio of the zero-dose to the maximum regenerative-dose); (3) the recycling ratio differed from unity by more than 2 sigma; (4) the DRC provided a poor fit to the L_x/T_x data points (i.e., the reduced chi squared value is larger than 5)(Peng and Li, 2017); and (5) the L_n/T_n value was statistically consistent (at 2σ) with or exceeded the saturation level of the corresponding DRC. Four or five discs (400 or 500 grains) were measured and at least 40 grains were accepted for each sample. Typical pIRIR T_n decay curve and DRC are shown in Fig. 4a and 4b for an accepted feldspar grain from sample YJG-07.

4 Results

To test the suitability of the single grain pIRIR procedure for our samples, residual dose and dose recovery tests were performed on one sample (YJG-07). In the tests, K-feldspar grains were first bleached for ~8 h using a Dr Hönle solar simulator (model: UVACUBE 400). Residual doses of the pIRIR signals were determined by measuring 200 bleached grains (2 discs) using the single-grain pIRIR procedure in Table 3. A total of 34 grains were accepted after applying the rejection criteria mentioned above and their residual doses are shown in Fig. 4d. We applied the Central Age Mode (CAM) (Galbraith et al., 1999) to estimate the weighted mean of residual dose, which yielded a value of 6.6 ± 0.7 Gy.

In the dose recovery test, a laboratory beta dose of ~35 Gy was given to 500 bleached grains (5 discs). The given dose was then measured as an 'unknown' dose using the procedure in Table 3. A total of 101 grains were accepted for dose determination after applying the criteria mentioned above. The distribution of recovered doses is shown in Fig. 4c. The dose recovery ratio (the ratio of measured to given dose) is 1.00 ± 0.03, after correcting residual dose. This result indicates that the given dose can be successfully recovered using the pIRIR procedure.

Anomalous fading tests were conducted on multi-grain single aliquots with two samples (YJG-04 and YJG-08) using a single aliquot procedure similar to that described by Auclair et al. (2003), but based on a pIRIR procedure. The results show that the two samples have similar anomalous fading rates (Fig. 5). The average *g*-values for the IRSL (200 °C) and pIRIR (275 °C) signals from the samples are 2.6 ± 0.3 and 0.3 ± 0.5 %/decade, respectively, indicating that the pIRIR signals suffer negligible anomalous fading.

Based on the performance tests described above, we used the single-grain pIRIR procedure to estimate the D_e values for the Yujiagou samples. The obtained pIRIR D_e distributions for all the samples are shown in Figs. 6 and 7, respectively. For the eight samples from lower layers (YJG-03–10), their over-dispersion (OD) values are between 17 and 28%, which are similar to those reported for well-bleached samples (Arnold et al., 2009; Arnold and Roberts, 2009). These OD values are consistent or slightly higher than the value obtained from dose recovery (~18%, Fig. 4c), which is expected as there are some additional dispersion from microdosimetry and unrecognised uncertainty in measuring natural signals (e.g., Galbraith and Roberts, 2012; Guérin et al., 2015). Most of the D_e values are randomly centred around the central values obtained using CAM, indicating that the deposits were sufficiently bleached prior to burial and there is no significant post-depositional mixture or disturbance for these layers. We, therefore, applied the CAM to calculate the final D_e values for these samples.

For the two topmost samples (YJG-01 and YJG-02), many feldspar grains yield D_e values close to zero (Fig. 6). These OD values are significantly higher than those of the lower samples (17 – 28%). Using CAM, the D_e values are 3.1 ± 0.3 and 3.0 ± 0.4 Gy and the corresponding OD are 152.0 ± 38.4 and 114.1 ± 46.4 %. As mentioned above, the grains with weak T_n signal were rejected by either the initial signal is less than 3 sigma above its background or its relative error is >25%, any grains with low signal brightness should not be accepted for D_e estimation. Hence, the presence of these modern or young feldspar grains can be explained by post-depositional mixing, supported by the field observation that Layer 1 is a disturbed layer with many vertical joints. In fact, the reason for the post-depositional mixing of the upper layers is most likely due to recent agricultural activities, which can be seen from the site where crop is still planted on the top surface. We, therefore, cannot provide reliable ages for these two samples. However, applying the Maximum Age Model (MAM) (Galbraith et al., 1999) allows us to constrain their minimum ages. To apply MAM, a σ_b value

representing the expected over-dispersion for a well-bleached and non-disturbed sample, is needed. We have used a σ_b value of 22% for our samples, based on the average OD values (17 to 28%) from the lower samples, in which no evidence of post-depositional mixture was observed. The MAM yielded maximum D_e values of 6.0 ± 0.4 Gy and 10.2 ± 2.2 Gy for YJG-01 and YJG-02, corresponding to the ages of 1.6 ± 0.1 ka and 2.7 ± 0.6 ka, respectively.

The presence of many zero-dose grains in the top samples indicates that the pIRIR signal of the K-feldspar grains of our samples can be sufficiently bleached prior to deposition and has negligible residual doses. We, therefore, did not make correction for residual doses when calculate the final D_e values for the other samples.

Ages for our samples were calculated by dividing the D_e values (MAM for YJG-01 and 02; CAM for others) by the total dose rates (Table 1, Fig. 8). The sample YJG-03 from bottom of Layer 2 was dated to 9.8 ± 0.6 ka. The four samples (YJG-04–07) from Layer 3a were dated from 9.7 ± 0.7 to 12.2 ± 0.7 ka, and three samples (YJG-08–10) collected from Layers 3b, 4 and 5 gave the ages of 12.8 ± 0.7 ka, 13.5 ± 0.9 ka and 13.5 ± 0.8 ka, respectively. The pIRIR ages are in stratigraphic order, further supporting that our samples were fully bleached prior to deposition.

5 Discussion

5.1 Revised chronologies

Fig. 8 summarises the revised luminescence chronology of the Yujiagou site based on single grain pIRIR age estimates, in comparison with previously age estimates provided by Xia et al. (2001) and Chen (1999). We did not show the two IRSL ages from Nagatomo et al. (2009) as the depths of their samples are not reported. The K-feldspar pIRIR ages of all our 10 samples are in stratigraphic order, increasing down-profile from layer 5 (13.5 ± 0.8 ka: YJG-10) to layer 1 (1.6 ± 0.1 ka: YJG-01). The age of Layer 3b (12.8 ± 0.7 ka) is consistent with the TL age (11.6 ka) obtained from a pottery fragment from the same layer (Chen, 1999), further supporting the reliability of our chronology.

Compared to the fine-grained quartz TL ages (Xia et al., 2001), our pIRIR ages are consistent with the TL ages for samples from the boundaries between Layers 1 and 2 and between Layers 6 and 7. The TL ages from Layers 2 and 3a, however, are underestimated, probably due to uncorrected sensitivity changes in TL measurements.

5.2 Paleoenvironmental implications

Xia et al. (2001) studied several climatic and environmental proxies, including fossil pollen assemblages, carbonate content, total organic carbon (TOC) and oxygen-carbon isotope of carbonate, for the Yujiagou section. Based on the proxy records, they divided the Yujiagou section into 4 stages (Fig. 8). According to our revised chronology, the four stages of climatic and environmental changes recorded in the Yujiagou section are described as follows.

5.2.1. Stage 4 (≥13.5 ka)

This stage corresponds to Layers 7–5. The age estimates (≥ 13.5 ka) suggest that these layers were deposited during the last glacial period. This is consistent with the evidence from climatic and environmental proxy records, characterised by low TOC values and a pollen assemblage dominated by herb indicating less dense boschveld condition. This stage also demonstrated the lowest ^{18}O values and highest ^{13}C values, suggesting a cold and dry climatic condition. Despite a cold and dry climate, the discovery of a few stone artifacts from these layers indicates that human activity was still presence in this region during this period.

5.2.2. Stage 3 (13.5 – 9.7 ka)

This stage is associated with layers 4–3a, dated from about 13.5 to 9.7 ka, so it belongs to the transitional period from the last deglaciation to the early Holocene. During this stage, herb predominates the pollen assemblage suggesting a temperate steppe or boschveld environment. This stage is also characterized by high values of ^{18}O and relative high value of ^{13}C, supporting a warm and dry condition during this period. Thousands of microliths were recovered, and polished stones and potteries firstly appeared, indicating that human activities became more intensified during this period.

5.2.3. Stage 2 (9.7 – ? ka)

This stage is associated with Layer 2, corresponding to Holocene period. Since the top of this layer was subjected to post-depositional mixture, the maximum pIRIR age (~2.7 ka) obtained for YJG-02 can only be regarded as a minimum estimate of the true depositional age, so the upper part of this layer was deposited at ~2.7 ka or probably slightly earlier. During this stage, herb was prevailing in the pollen assemblage, but the amount of woody plants and fern spores increased, which indicates a temperate forest steppe environment. This stage is characterized by high TOC, relatively high ^{18}O, the lowest ^{13}C, suggesting that this period was warm and humid. A total of 389 chipped stone artefacts, 11 polished stone artefacts, 27 pottery shards and three ornaments were discovered from this layer.

5.2.4. Stage 1 (< 1.6 ka)

This stage is associated with Layer 1, which was significantly affected by post-depositional mixture, as indicated by pIRIR results of YJG-01. Given this reason, we can only tentatively assign the maximum age estimate of YJG-01 (~1.6 ka) as the true depositional age of its bottom part. Herb still maintains its previous dominant level in this pollen assemblage, and fern spores increase progressively. This stage is characterized by high ^{18}O and ^{13}C values, indicating a warm and dry (compare to stage 2) climate, which is also supported by the relatively high TOC values. These indicate that the local environment was a relatively temperate forest steppe with a warm and damp climatic condition.

We have summarised the paleoclimate reconstructed from the Yujiagou section in Fig. 9, with comparison with those obtained from other regions in northern China (Fig. 1a), including Daihai lake (Xiao et al., 2004), Mu Us Desert (Sun et al., 2006), and Hani peat bog (Seki et al., 2009; Zhou et al., 2010). It is shown that the Holocene climate in the Nihewan Basin is not completely consistent with those for other localities in north-central China. This may indicate that the Holocene climate evolution in north-central China was a regional phenomenon, and the East Asian monsoon variably affected different regions at different time scales (Cai et al., 2010; Liu et al., 2015; Zou et al., 2018).

5.3 Archaeological implications

Microliths were discovered in the Yujiagou site from Layers 7–2, dated to 13.5–9.7 ka. The earliest microblade in the Nihewan Basin was found in the Zhiyu site (dated to 31–39 ka) (Institute of Archaeology, 1991; Yuan, 1993), and typical microblade was found at the Youfang site (dated to 26–29 ka) (Nian et al., 2014) (Fig. 1b). Further study of the characteristics of the microliths in the Yujiagou and the comparison with the former two sites is necessary to provide more information about timeline of stone techniques development in this region.

Potteries (three shards) were first discovered in Layer 4 (~13 ka), and was found continuously up to Layer 2 (~9.7 ka), where microblades and animal bones were significantly reduced. The polished

stones also appeared together with the pottery. Both the potteries and polished stones in the Yujiagou are oldest in the Nihewan Basin, although they were also found in the Heitupou site (~7.5 ka) and the Jiangjialiang site (~6.8 ka) at this region (Xie et al., 2006).

The production of polished stone has been regarded as a millstone of Neolithic stage, because it can be used to process plant resources, such as cereals, acorns, or roots, by rubbing and grinding (Wright, 1994; Fullagar and Field, 1997). Pottery can be used for food preparation, storage, cooking (starch-rich food and meat) and extraction of marrow and grease (Hayden, 2003; Carmody et al., 2011; Prendergast et al., 2009). So, the appearance of pottery and polished stones in the Yujiagou site at ~13 ka ago indicates better utilize existing resources by consuming foods that are hard to process and digest and by more efficient extraction of their nutritional elements (Shelach, 2012; Stiner, 2001). Extraction of plant starch grains from the polished stones and potteries in Yujiagou and use-wear analyses are necessary for further investigation about the diet of ancient human and the transition process from the Paleolithic to Neolithic culture in the Nihewan Basin.

Our new dating results, together with the paleoenvironmental record, suggest that the polished stones and pottery sherds appeared when the climate became warmer. It is interesting that in Yujiagou the change from Paleolithic to Neolithic are associated with a period of slightly humid (compare with Stage 4) and warmer climate with less survival stress. Besides, the zooliths were hardly found in Layer 2, indicating that gathering and food processing might had substituted hunting as primary modes of living and production at that time and the change of living and production mode resulted in an advancement of tools and cultural development (Xia et al., 2001).

6 Conclusions

The age of the Yujiagou site in the Nihewan Basin of northern China have been reinvestigated in this study using pIRIR dating procedure for single grains of K-feldspar. Our results suggest that the cultural layers at Yujiagou site were deposited during 13.5–9.7 ka. Our ages also indicate that the polished stones and potteries started from ~13 ka in this site, corresponding to a warm and dry condition. The appearance of these new technologies may imply an exploitation of a wider range of plants and benefit to their domestication. Further investigations, including extracting plant starch and animal proteins from potteries and grinding stones and use-wear studies, are necessary for better understanding the diet of ancient human populations and the transition process from the Paleolithic to Neolithic culture in the Nihewan Basin.

Acknowledgements

This study was supported by an Australian Research Council Future Fellowship to Bo Li (FT140100384), grants from the National Natural Science Foundation of China to Jiafu Zhang (NSFC, No. 41471003) and Yujie Guo (No. 41702192) and postgraduate scholarships from the China Scholarship Council and the University of Wollongong to Xue Rui (201506010345). We thank Weiwen Huang, Yongming Meng, Qi Wei, Shengquan Cheng and Fagang Wang for helps with the field investigations and collection of OSL samples. Kieran O'Gorman and Mariana Sontag Gonzalez provided helps in the measurement of internal K contents. Richard G. Roberts, Zenobia Jacobs, Yasaman Jafari and Terry Lachlan gave valuable support in the OSL dating laboratory. Two anonymous reviewers provided constructive suggestions and comments to the manuscript.

REFERENCE

Aitken MJ. (1985) *Thermoluminescence dating*: Academic press.
Aitken MJ. (1998) *Introduction to optical dating: the dating of Quaternary sediments by the use of photon-stimulated luminescence*: Clarendon Press.
Arnold LJ and Roberts RG. (2009). Stochastic modelling of multi-grain equivalent dose (D-e) distributions: Implications for OSL dating of sediment mixtures. *Quaternary Geochronology* 4: 204–230.
Arnold LJ, Roberts RG, Galbraith RF, et al. (2009). A revised burial dose estimation procedure for optical dating of young and modern-age sediments. *Quaternary Geochronology* 4: 306–325.
Auclair M, Lamothe M and Huot S. (2003) Measurement of anomalous fading for feldspar IRSL using SAR. *Radiation Measurements* 37: 487-492.
Blegen N, Tryon CA, Faith JT, et al. (2015) Distal tephras of the eastern Lake Victoria basin, equatorial East Africa: correlations, chronology and a context for early modern humans. *Quaternary Science Reviews* 122: 89-111.
Bøtter-Jensen L, Andersen CE, Duller GAT, et al. (2003) Developments in radiation, stimulation and observation facilities in luminescence measurements. *Radiation Measurements* 37: 535-541.
Bøtter-Jensen L, Bulur E, Duller G, et al. (2000) Advances in luminescence instrument systems. *Radiation Measurements* 32: 523-528.
Cai Y, Tan L, Cheng H, et al. (2010) The variation of summer monsoon precipitation in central China since the last deglaciation. *Earth and Planetary Science Letters* 291: 21-31.
Carmody RN, Weintraub GS and Wrangham RW. (2011) Energetic consequences of thermal and nonthermal food processing. *Proceedings of the National Academy of Sciences* 108: 19199-19203.
Chen X. (1999) Discovery on the early neolithic culture in China -- Issues of the earliest pottery. In: Xu Q, Xie F and Wang J (eds) *New Advance of Archaeology in Prehesitory.* Beijing: Science Press, 189-202.
Fullagar R and Field J. (1997) Pleistocene seed-grinding implements from the Australian arid zone. *Antiquity* 71: 300-307.
Galbraith RF and Roberts RG. (2012) Statistical aspects of equivalent dose and error calculation and display in OSL dating: An overview and some recommendations. *Quaternary Geochronology* 11: 1-27.
Galbraith RF, Roberts RG, Laslett GM, et al. (1999) OPTICAL DATING OF SINGLE AND MULTIPLE GRAINS OF QUARTZ FROM JINMIUM ROCK SHELTER, NORTHERN AUSTRALIA: PART I, EXPERIMENTAL DESIGN AND STATISTICAL MODELS*. *Archaeometry* 41: 339-364.
Guérin G, Jain M, Thomsen KJ, et al. (2015) Modelling dose rate to single grains of quartz in well-sorted sand samples: The dispersion arising from the presence of potassium feldspars and implications for single grain OSL dating. *Quaternary Geochronology* 27: 52-65.
Guo Y-J, Li B, Zhang J-F, et al. (2016) Luminescence ages for three 'Middle Palaeolithic' sites in the Nihewan Basin, northern China, and their archaeological and palaeoenvironmental implications. *Quaternary Research* 85: 456-470.
Guo YJ, Li B, Zhang JF, et al. (2017) New ages for the Upper Palaeolithic site of Xibaimaying in the Nihewan Basin, northern China: implications for small‐tool and microblade industries in north‐east Asia during Marine Isotope Stages 2 and 3. *Journal of Quaternary Science* 32: 540-552.
Guralnik B, Li B, Jain M, et al. (2015) Radiation-induced growth and isothermal decay of infrared-stimulated luminescence from feldspar. *Radiation Measurements* 81: 224-231.
Hayden B. (2003) Were luxury foods the first domesticates? Ethnoarchaeological perspectives from Southeast Asia. *World Archaeology* 34: 458-469.
Huntley DJ, Godfrey-Smith DI and Thewalt ML. (1985) Optical dating of sediments. *Nature* 313: 105.
Huntley DJ and Hancock RGV. 2001. The Rb contents of the K-feldspars being measured in optical dating. Ancient TL 19: 43–46.

Institute of Archaeology C. (1991) Radiocarbon Dates in Chinese Archaeology (1965-1991). . Cultural Relics Publishing House, Beijing (in Chinese).
Jacobs Z, Duller GAT and Wintle AG. (2006) Interpretation of single grain De distributions and calculation of De. *Radiation Measurements* 41: 264-277.
Jacobs Z, Meyer MC, Roberts RG, et al. (2011) Single-grain OSL dating at La Grotte des Contrebandiers ('Smugglers' Cave'), Morocco: improved age constraints for the Middle Paleolithic levels. *Journal of Archaeological Science* 38: 3631-3643.
Jacobs Z and Roberts RG. (2007) Advances in optically stimulated luminescence dating of individual grains of quartz from archeological deposits. *Evolutionary Anthropology: Issues, News, and Reviews* 16: 210-223.
Kreutzer S, Schmidt C, Fuchs MC, et al. (2012) Introducing an R package for luminescence dating analysis. *Ancient TL* 30: 1-8.
Li B and Li S-H. (2011) Luminescence dating of K-feldspar from sediments: A protocol without anomalous fading correction. *Quaternary Geochronology* 6: 468-479.
Liu J, Chen J, Zhang X, et al. (2015) Holocene East Asian summer monsoon records in northern China and their inconsistency with Chinese stalagmite δ18O records. *Earth-Science Reviews* 148: 194-208.
Mei H. (2007) Transition from Paleolithic to Neolithic in the Nihewan Basin: A study of the discoveries from Yujiagou site. *Unpublished PhD Dissertation, Department of Archaeology, Peking University.(in Chinese)*.
Murray AS and Wintle AG. (2000) Luminescence dating of quartz using an improved single-aliquot regenerative-dose protocol. *Radiation Measurements* 32: 57-73.
Nagatomo T, Shitaoka Y, Namioka H, et al. (2009) OSL dating of the strata at Paleolithic sites in the Nihewan Basin, China. *Acta Anthropologica Sinica* 28: 276-284.
Nian X, Gao X, Xie F, et al. (2014) Chronology of the Youfang site and its implications for the emergence of microblade technology in North China. *Quaternary International* 347: 113-121.
Peng J, Dong Z, Han F, et al. (2013) R package numOSL: numeric routines for optically stimulated luminescence dating. Ancient TL 31: 41-48.
Peng J and Li B. (2017) Single-aliquot Regenerative-Dose (SAR) and Standardised Growth Curve (SGC) Equivalent Dose Determination in a Batch Model Using the R Package 'numOSL'. *Ancient TL* 35: 32-53.
Prendergast ME, Yuan J and Bar-Yosef O. (2009) Resource intensification in the Late Upper Paleolithic: a view from southern China. *Journal of Archaeological Science* 36: 1027-1037.
Prescott JR and Hutton JT. (1994) Cosmic ray contributions to dose rates for luminescence and ESR dating: Large depths and long-term time variations. *Radiation Measurements* 23: 497-500.
R Core Team. (2016) R: A language and environment for statistical computing. Vienna, Austria.
Roberts RG, Jacobs Z, Li B, et al. (2015) Optical dating in archaeology: thirty years in retrospect and grand challenges for the future. *Journal of Archaeological Science* 56: 41-60.
Rui X, Li B, Guo YJ, et al. (2018) Variability in the thermal stability of OSL signal of single-grain quartz from the Nihewan Basin, North China. *Quaternary Geochronology*.
Seki O, Meyers PA, Kawamura K, et al. (2009) Hydrogen isotopic ratios of plant wax n-alkanes in a peat bog deposited in northeast China during the last 16kyr. *Organic Geochemistry* 40: 671-677.
Shelach G. (2012) On the invention of pottery. *Science* 336: 1644-1645.
Stiner MC. (2001) Thirty years on the "Broad Spectrum Revolution" and paleolithic demography. *Proceedings of the National Academy of Sciences* 98: 6993-6996.
Sun J, Li S-H, Han P, et al. (2006) Holocene environmental changes in the central Inner Mongolia, based on single-aliquot-quartz optical dating and multi-proxy study of dune sands. *Palaeogeography, Palaeoclimatology, Palaeoecology* 233: 51-62.

492 Thomsen KJ, Murray AS, Jain M, et al. (2008) Laboratory fading rates of various luminescence signals
493 from feldspar-rich sediment extracts. *Radiation Measurements* 43: 1474-1486.
494 Wright KI. (1994) Ground-stone tools and hunter-gatherer subsistence in southwest Asia:
495 implications for the transition to farming. *American Antiquity* 59: 238-263.
496 Xia Z, Chen F, Chen G, et al. (2001) Environmental background of evolution from the paleolithic to
497 neolithic culture in Nihewan Basin, North China. *Science in China Series D: Earth Sciences* 44:
498 779-788.
499 Xiao J, Xu Q, Nakamura T, et al. (2004) Holocene vegetation variation in the Daihai Lake region of
500 north-central China: a direct indication of the Asian monsoon climatic history. *Quaternary*
501 *Science Reviews* 23: 1669-1679.
502 Xie F, Li J and Liu L. (2006) Paleolithic archeology in the Nihewan Basin. *Huashan Literature & Arts*
503 *Press, Shijiazhuang, China*: 278.
504 Yuan S. (1993) AMS radiocarbon dating of Xinglong carved antler, Shiyu and Ximiao sites. *Acta*
505 *Anthropologica Sinica* 12: 92-95.
506 Zhou W, Zheng Y, Meyers PA, et al. (2010) Postglacial climate-change record in biomarker lipid
507 compositions of the Hani peat sequence, Northeastern China. *Earth and Planetary Science*
508 *Letters* 294: 37-46.
509 Zou G-N, Shelach G, Li X-Q, et al. (2018) Geochronology and paleoenvironment of the Taoshan site,
510 northeastern China, and archaeological implications. *Quaternary International* 463: 6-17.

511

Table 1

Dose rates, D_e values and ages for sediment samples from the Yujiagou site.

Sample	Depth, m	U, ppm	Th, ppm	K, %	Environmental dose rate, Gy/ka [a]					Accepted/ measured grains	D_e, Gy	Age, ka [b]
					External			Internal	Total			
					Gamma	Beta	Cosmic					
Layer 1												
YJG-01	0.3	3.65 ± 0.16	8.0 ± 1.2	1.89	1.08 ± 0.08	1.63 ± 0.11	0.21 ± 0.03	0.85 ± 0.14	3.77 ± 0.18	90/500	6.0 ± 0.4	1.6 ± 0.1
Layer 2												
YJG-02	0.7	3.15 ± 0.13	8.48 ± 1.07	1.95	1.07 ± 0.07	1.63 ± 0.11	0.19 ± 0.03	0.85 ± 0.14	3.74 ± 0.18	71/500	10.2 ± 2.2	2.7 ± 0.6
YJG-03	1.5	3.74 ± 0.15	6.49 ± 1.04	1.96	1.04 ± 0.07	1.65 ± 0.10	0.17 ± 0.03	0.85 ± 0.15	3.71 ± 0.18	77/500	36.5 ± 1.4	9.8 ± 0.6
Layer 3a												
YJG-04	1.9	3.94 ± 0.17	8.15 ± 1.24	2.00	1.13 ± 0.08	1.71 ± 0.10	0.17 ± 0.03	0.85 ± 0.14	3.86 ± 0.18	40/400	37.5 ± 2.0	9.7 ± 0.7
YJG-05	2.3	3.72 ± 0.13	5.28 ± 0.90	2.03	1.01 ± 0.07	1.68 ± 0.10	0.16 ± 0.02	0.85 ± 0.14	3.70 ± 0.18	102/500	42.0 ± 1.2	11.4 ± 0.7
YJG-06	2.6	3.51 ± 0.15	7.69 ± 1.15	2.01	1.07 ± 0.08	1.66 ± 0.10	0.16 ± 0.02	0.85 ± 0.14	3.74 ± 0.18	76/500	50.2 ± 1.4	13.4 ± 0.8
YJG-07	3.0	4.04 ±0.13	5.41 ± 0.87	2.01	1.05 ± 0.07	1.72 ± 0.10	0.15 ± 0.02	0.85 ± 0.14	3.77 ± 0.18	74/500	46.1 ± 1.3	12.2 ± 0.7
Layer 3b												
YJG-08	3.6	4.03 ± 0.14	5.52 ±0.94	2.02	1.04 ± 0.07	1.68 ± 0.10	0.14 ± 0.02	0.85 ± 0.14	3.71 ± 0.18	85/500	47.6 ± 1.1	12.8 ± 0.7
Layer 4												
YJG-09	5.0	4.19 ± 0.17	7.70 ± 1.20	1.76	1.06 ± 0.08	1.61 ± 0.10	0.13 ± 0.02	0.85 ± 0.14	3.65 ± 0.18	51/400	49.4 ± 1.8	13.5 ± 0.9
Layer 5												
YJG-10	5.8	4.61 ±0.18	8.65 ± 1.28	1.79	1.13 ± 0.08	1.69 ± 0.10	0.12 ± 0.02	0.85 ± 0.14	3.79 ± 0.18	82/400	51.3 ± 1.3	13.5 ± 0.8

[a] The external dose rates were corrected for water attenuation by a water content of 15 ± 5%.

[b] A relative error of 2% was included in the uncertainty on the final ages to allow for possible bias in the calibration of the laboratory beta source

Table 2

SEM results of internal K concentrations for 21 K-feldspar grains from sample YJG-08.

Grain	Point	K %	Na %	Ca %	Total % [a]	Corrected K % [a]
Grain 1	point 1	8.77	1.29	0.12	77.98	11.25
	point 2	8.78	1.01	0.1	74.72	11.75
Grain 2	point 1	9.27	1	0.11	78.16	11.86
	point 2	8.81	1.07	0.1	75.61	11.65
Grain 3	point 1	9.25	0.99	0.19	78.46	11.79
	point 2	9.14	0.92	0.14	76.53	11.94
Grain 4	point 1	8.97	1.1	0.17	77.58	11.56
	point 2	9.06	0.99	0.26	77.59	11.68
Grain 5	point 1	9.18	0.64	0.07	73.14	12.55
	point 2	9.53	0.67	0	75.48	12.63
Grain 6	point 1	9.25	0.85	0.09	76.17	12.14
	point 2	9.25	0.75	0.19	75.72	12.22
Grain 7	point 1	8.85	1.18	0.13	77.36	11.44
Grain 8	point 1	9.57	0.62	0.17	76.38	12.53
	point 2	9.68	0.77	0.14	78.66	12.31
Grain 9	point 1	9.37	0.8	0	75.83	12.36
	point 2	9.3	0.69	0.26	75.88	12.26
Grain 10	point 1	9.46	0.75	0.14	76.87	12.31
	point 2	9.12	0.63	0.18	73.36	12.43
Grain 11	point 1	9.1	0.98	0	75.96	11.98
	point 2	9.04	1.05	0	76.33	11.84
Grain 12	point 1	9.16	0.9	0	75.47	12.14
Grain 13	point 1	9.44	0.75	0.1	76.45	12.35
Grain 14	point 1	9.56	0.84	0.07	78.12	12.24
Grain 15	point 1	9.47	0.83	0.09	77.51	12.22
Grain 16	point 1	9.54	0.86	0.11	78.49	12.16
	point 2	9.47	0.79	0.19	77.74	12.18
Grain 17	point 1	9.52	0.83	0.18	78.49	12.13
Grain 18	point 1	9.21	1.08	0.13	78.78	11.69
	point 2	9.25	0.93	0.24	78.12	11.84
Grain 19	point 1	9.43	0.94	0.05	78.20	12.06
Grain 20	point 1	9.16	0.96	0.12	76.99	11.90
	point 2	9.6	0.76	0.1	77.70	12.35
Grain 21	point 1	9.51	0.66	0	75.23	12.64
	point 2	9.43	0.7	0.14	76.09	12.39

[a] Total % represent the sum of the weight concentration percentage of $KAlSi_3O_8$, $NaAlSi_3O_8$, and $CaAl_2Si_2O_8$ in each grain, based on the measured result of K%, Na% and Ca% by the Phenom XL Scanning Election Microscope (SEM), respectively. As $KAlSi_3O_8$, $NaAlSi_3O_8$, and $CaAl_2Si_2O_8$ should makes up 100% for feldspar, the lower total percentage is a result of background signal of oxygen from resin that was used to mount grains for measurements. As a result, the K % has been corrected for the loss in total percentage.

Table 3

The single-grain post-infrared infrared stimulated luminescence (pIRIR) measurements.

Step	Treatment	Signal
1	Give regenerative dose, D_i	
2	Preheat at 320 °C for 60 s	
3	IRSL measurement at 200 °C for 200 s	
4	SG IRSL measurement at 275 °C for 1.5 s	$L_{x(275)}$
5	Give test dose, D_t	
6	Preheat at 320 °C for 60 s	
7	IRSL measurement at 200 °C for 200 s	
8	SG IRSL measurement at 275 °C for 1.5 s	$T_{x(275)}$
9	IR bleach at 340 °C for 100 s	
10	Return to step 1	

Figures' captions

Fig. 1. (a) Map showing the locations of the Nihewan Basin (red rectangle), Daihai lake, Mu Us Desert (MU) and Hani bog mentioned in the text. (b) DEM map showing the Nihewan Basin (dasheed line), the Sanggan River and the archaeological sites with microblade tools.

Fig. 2. Photograph of the west section of Yujiaghou_A showing the stratigraphy and the position of dating samples.

Fig. 3. Drawing of stone artefacts at Yujiagou (from Mei, 2007): (a) stone axe (no. 3: 259), (b) conical microcore (no. 3: 10), (c) spall (no. 3: 134), and (d) stone mill (no. A4: 7).

Fig. 4. (a) pIRIR decay curve for one feldspar grain from sample YJG-07. (b) The dose response curve for the same grain. The solid squares represent the sensitivity-corrected regenerative signals (L_x/T_x). The open squares represent the sensitivity-corrected natural signal (L_n/T_n). The data points are fitted using a general-order kinetic (GOK) function of the form $I = a*[1-(1+b*c*x)^{(-1/c)}]+d$, where x is the regenerative dose and parameters a, b, c and d are constants. D_e is obtained by projecting the L_n/T_n onto the fitted curve and interpolating the dose axis (dashed lines). (c) Equivalent dose (D_e) values for 101 accepted grains of sample YJG-07 that had been optically bleached and given a known beta dose of 35 Gy. The shaded region indicates the 2σ range from the weighted mean calculated using Central Age Model (CAM). (d) Distribution of residual dose values for all accepted grains of the same sample.

Fig. 5. Anomalous fading results of the IRSL and pIRIR signals from samples YJG-04 (a) and YJG-08 (b). t is delayed period and t_c is calculated as the time from the middle point of irradiation and the beginning of measurement. The g-values of these two samples are summarized in (c).

Fig. 6. Histogram summarising the D_e distribution for the accepted grains from (a) YJG-01 and (b) YJG-02. (c) and (d) are the corresponding radial plots of these two samples. The red lines indicate the D_e results obtained using the maximum age model.

Fig. 7. (a)–(h) D_e distribution for the accepted grains of samples YJG-03–10, respectively. The shaded region indicates the 2σ range from the weighted mean calculated using CAM.

Fig. 8. Diagram of feldspar single-grain ages, fine quartz single aliquot TL (Xia et al., 2001) and pottery TL (Chen, 1999) ages, lithology sequence, main sporopollen percentage, oxygen and carbon isotopic records, and $CaCO_3$ and TOC contents in the Yujiagou site (modified after Xia et al., 2001). The dotted black lines in (a) shows the boundaries between different layers. The dashed blue lines in (c) – (j) shows the boundaries between different stages.

Fig. 9. Comparison of the climate histories of the study region and other localities in north China, including Daihai Lake (Xiao et al., 2004), Mu Us Desert (Sun et al., 2006), and Hani peat bog (Seki et al., 2009; Zhou et al., 2010). The solid lines represents periods with firm chronology, and the dashed lines represents periods where age ranges are not firmly established. The question marks indicate unknown ages.

Fig. 1.

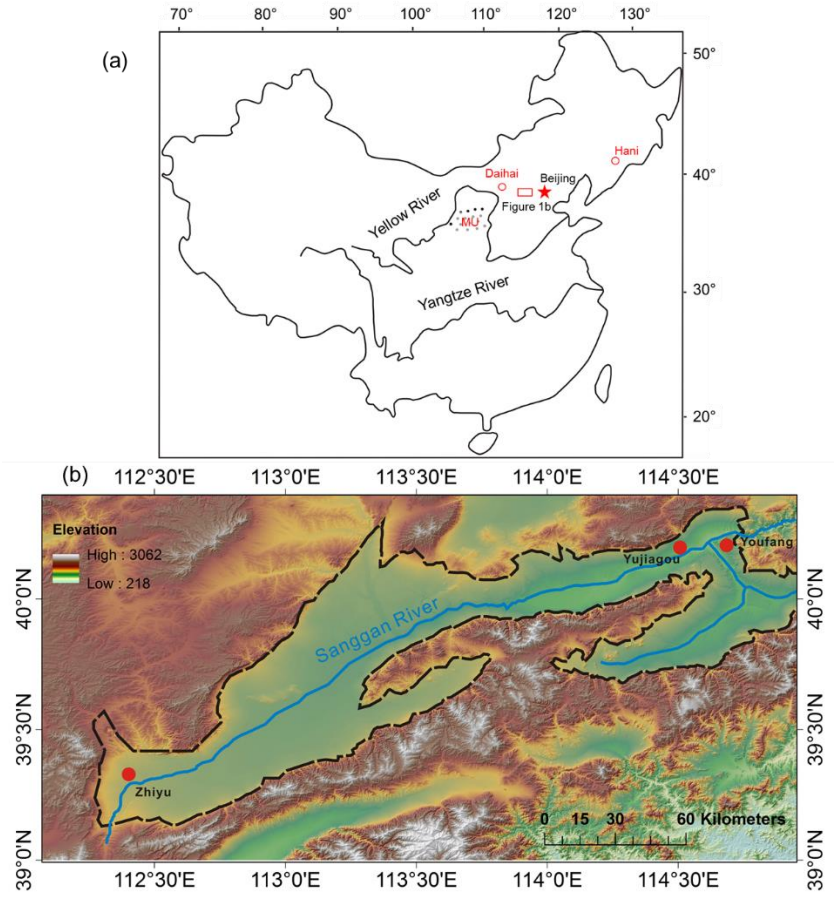
(a)
70°
80°
90°
100°
110°
120°
130°
50°
40°
30°
20°
Hani
Daihai
Beijing
Figure 1b
MU
Yellow River
Yangtze River
(b)
112°30'E
113°0'E
113°30'E
114°0'E
114°30'E
Elevation
High : 3062
Low : 218
Yujiagou
Youfang
Sanggan River
Zhiyu
0 15 30 60 Kilometers
40°0'N
39°30'N
39°0'N

Fig. 2.

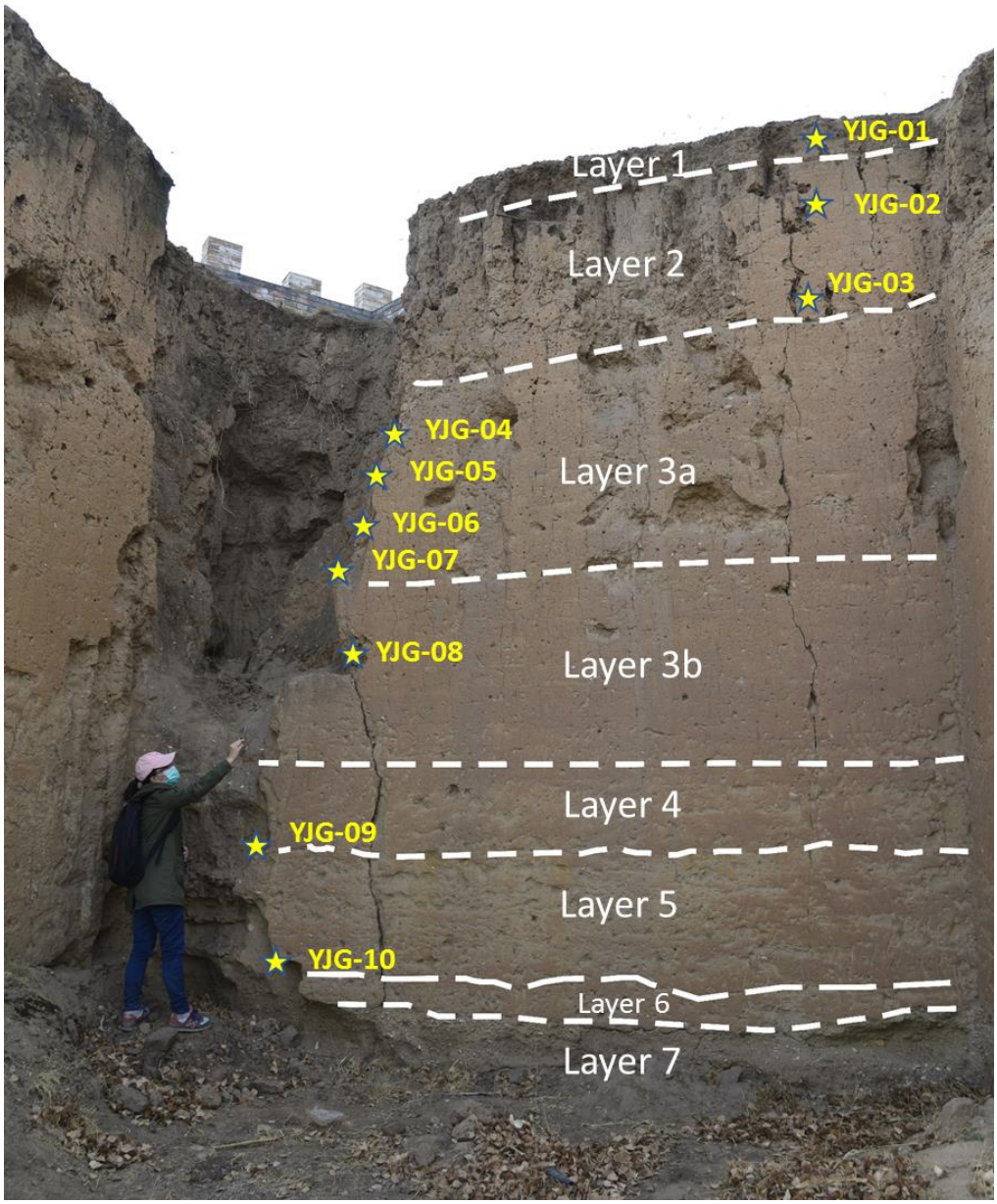
YJG-01
Layer 1
YJG-02
Layer 2
YJG-03
YJG-04
YJG-05
Layer 3a
YJG-06
YJG-07
YJG-08
Layer 3b
Layer 4
YJG-09
Layer 5
YJG-10
Layer 6
Layer 7

Fig. 3.

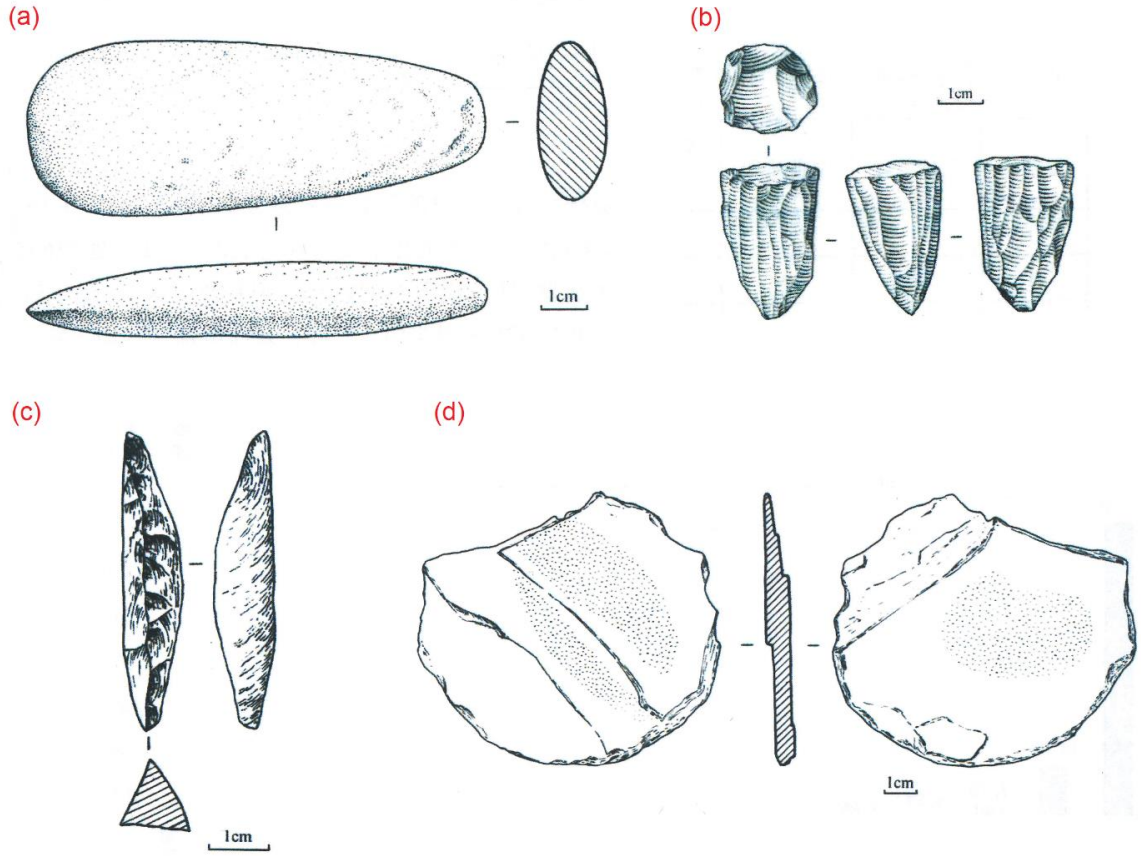

Fig.4.

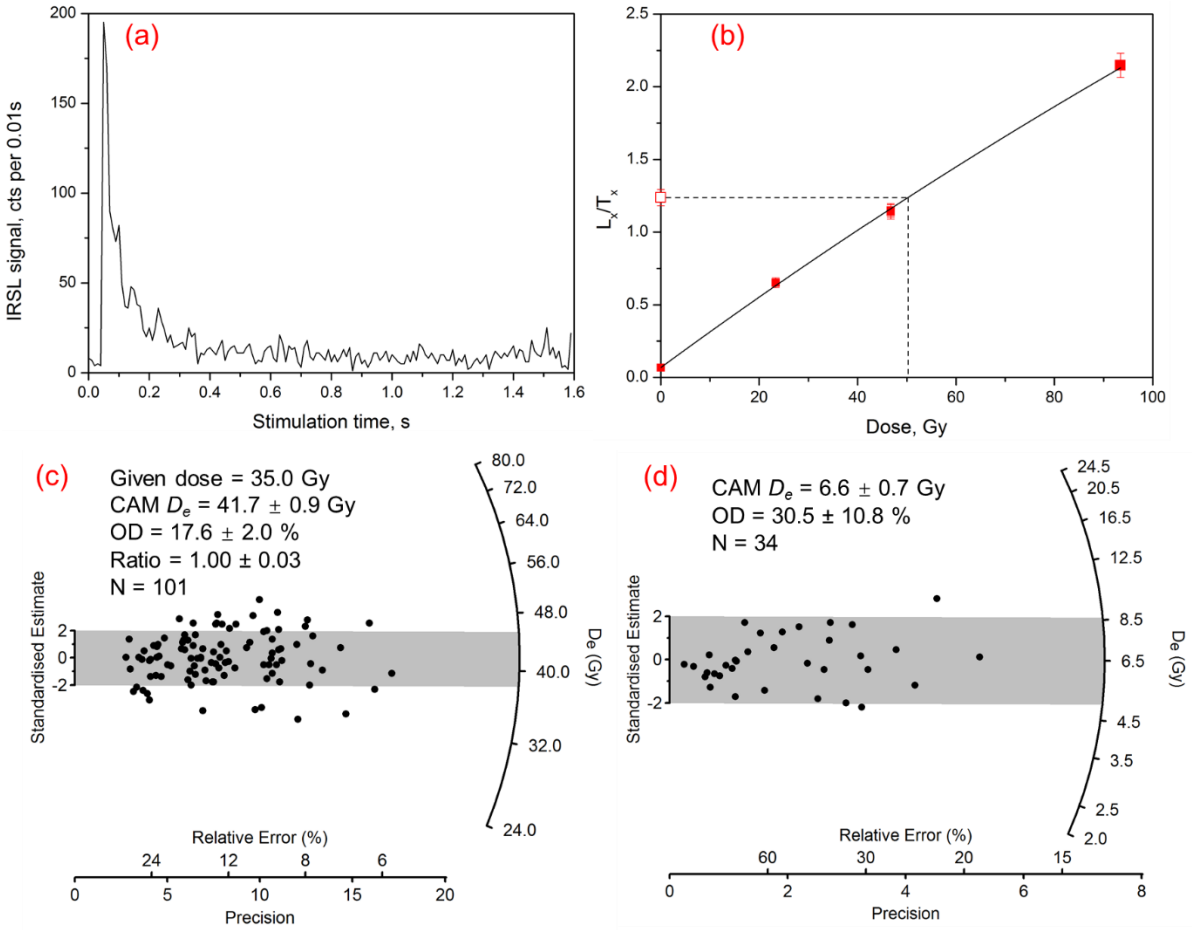
(a)
IRSL signal, cts per 0.01s
Stimulation time, s
(b)
L_x/T_x
Dose, Gy
(c)
Given dose = 35.0 Gy
CAM D_e = 41.7 ± 0.9 Gy
OD = 17.6 ± 2.0 %
Ratio = 1.00 ± 0.03
N = 101
Standardised Estimate
De (Gy)
Relative Error (%)
Precision
(d)
CAM D_e = 6.6 ± 0.7 Gy
OD = 30.5 ± 10.8 %
N = 34
Standardised Estimate
De (Gy)
Relative Error (%)
Precision

Fig. 5.

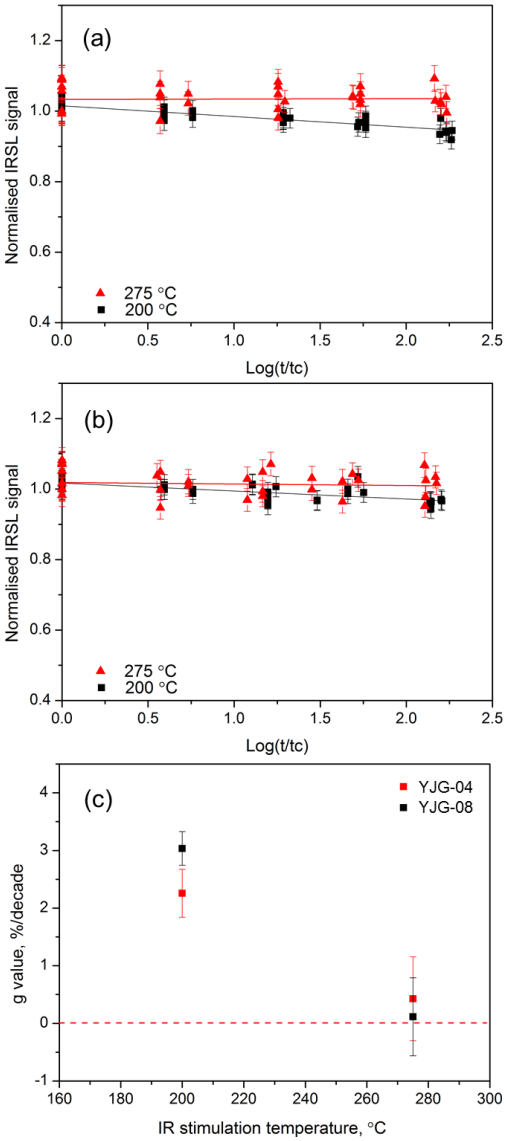
(a)
Normalised IRSL signal
275 °C
200 °C
Log(t/tc)
(b)
Normalised IRSL signal
275 °C
200 °C
Log(t/tc)
(c)
YJG-04
YJG-08
g value, %/decade
IR stimulation temperature, °C

Fig. 6.

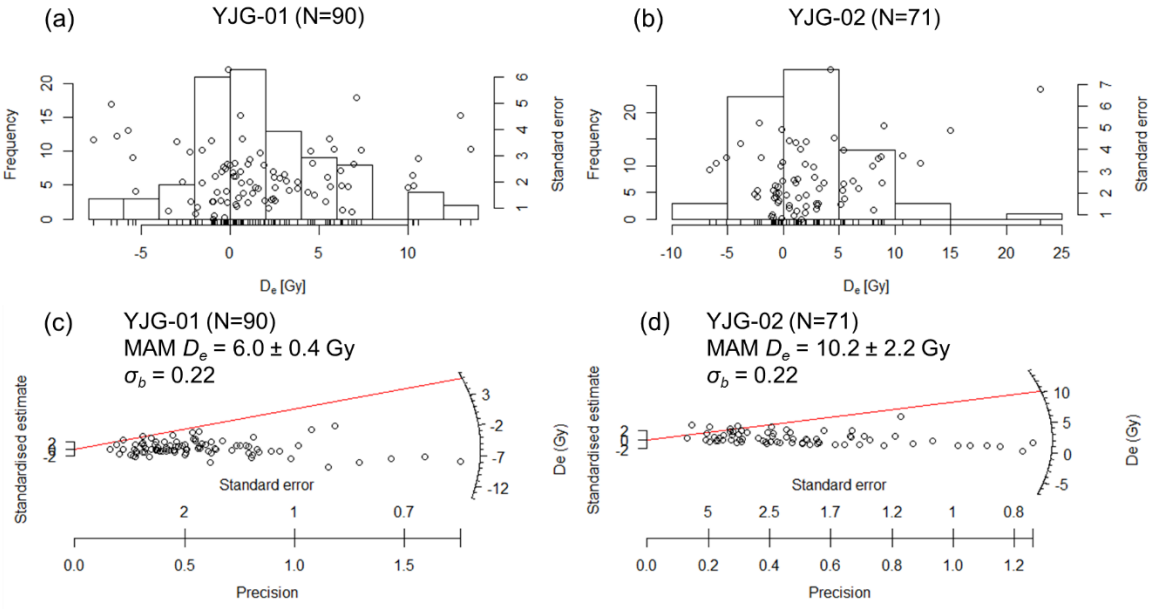
(a)
YJG-01 (N=90)
Frequency
Standard error
De [Gy]
(b)
YJG-02 (N=71)
Frequency
Standard error
De [Gy]
(c)
YJG-01 (N=90)
MAM De = 6.0 ± 0.4 Gy
σb = 0.22
Standardised estimate
Standard error
Precision
(d)
YJG-02 (N=71)
MAM De = 10.2 ± 2.2 Gy
σb = 0.22
Standardised estimate
De (Gy)
Standard error
Precision

Fig. 7.

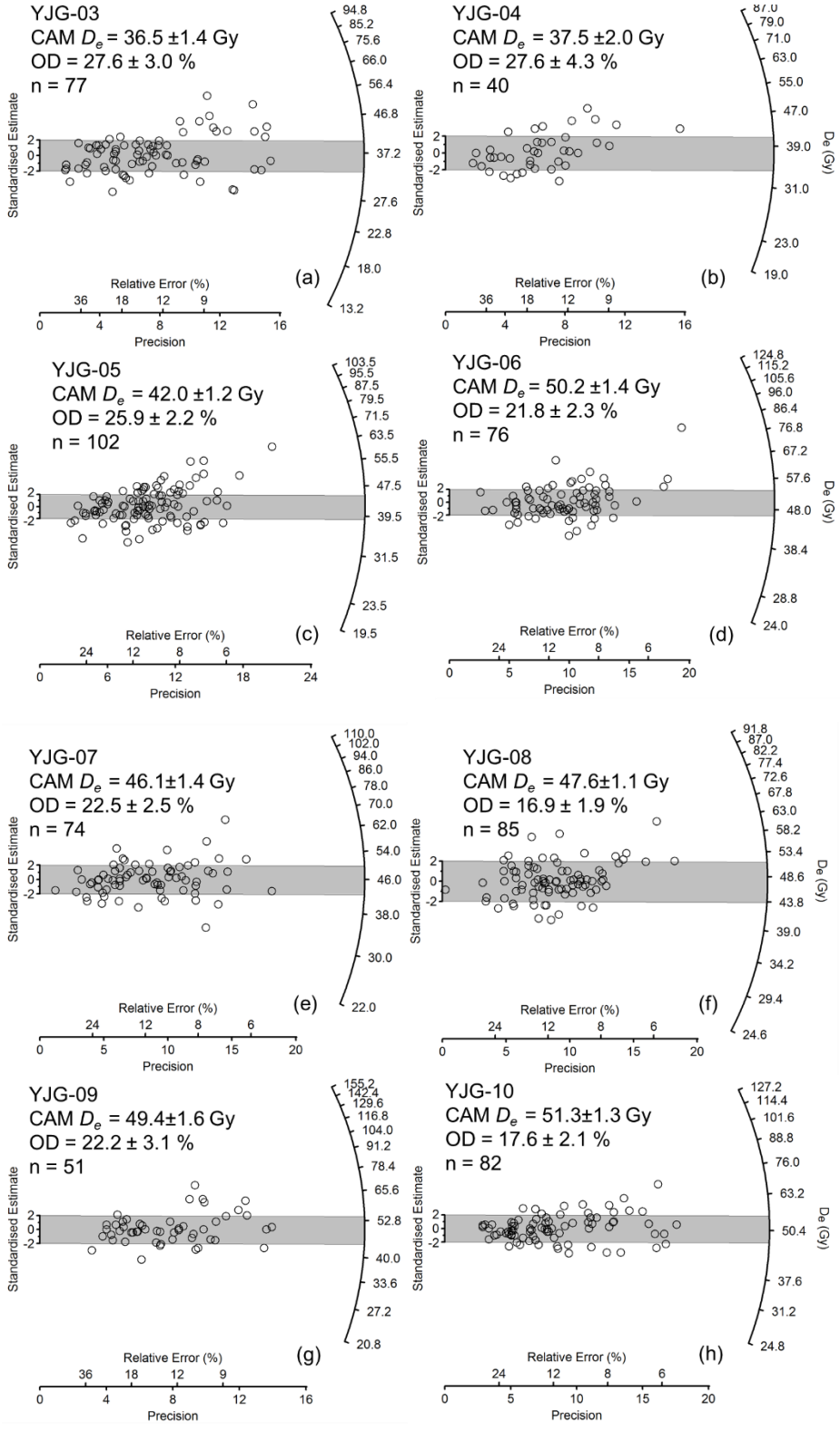
YJG-03
CAM D_e = 36.5 ±1.4 Gy
OD = 27.6 ± 3.0 %
n = 77
(a)
YJG-04
CAM D_e = 37.5 ±2.0 Gy
OD = 27.6 ± 4.3 %
n = 40
(b)
YJG-05
CAM D_e = 42.0 ±1.2 Gy
OD = 25.9 ± 2.2 %
n = 102
(c)
YJG-06
CAM D_e = 50.2 ±1.4 Gy
OD = 21.8 ± 2.3 %
n = 76
(d)
YJG-07
CAM D_e = 46.1±1.4 Gy
OD = 22.5 ± 2.5 %
n = 74
(e)
YJG-08
CAM D_e = 47.6±1.1 Gy
OD = 16.9 ± 1.9 %
n = 85
(f)
YJG-09
CAM D_e = 49.4±1.6 Gy
OD = 22.2 ± 3.1 %
n = 51
(g)
YJG-10
CAM D_e = 51.3±1.3 Gy
OD = 17.6 ± 2.1 %
n = 82
(h)
Standardised Estimate
Relative Error (%)
Precision
De (Gy)

Fig. 8.

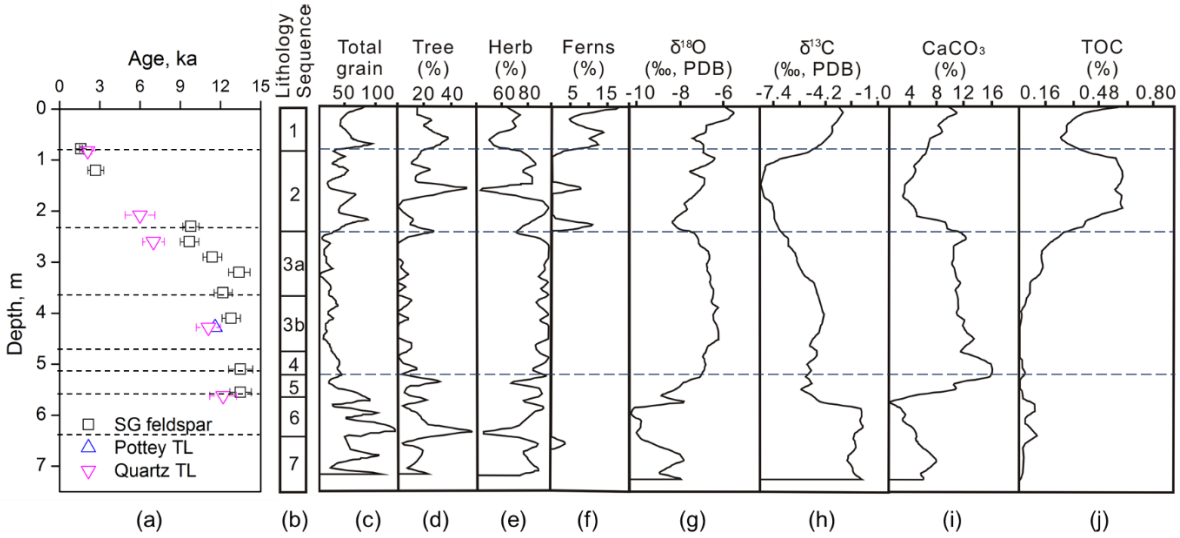
Age, ka
0 3 6 9 12 15
Depth, m
0 1 2 3 4 5 6 7
SG feldspar
Pottey TL
Quartz TL
Lithology Sequence
1
2
3a
3b
4
5
6
7
Total grain
50 100
Tree (%)
20 40
Herb (%)
60 80
Ferns (%)
5 15
δ18O (‰, PDB)
-10 -8 -6
δ13C (‰, PDB)
-7.4 -4.2 -1.0
CaCO3 (%)
4 8 12 16
TOC (%)
0.16 0.48 0.80
(a)
(b)
(c)
(d)
(e)
(f)
(g)
(h)
(i)
(j)

Fig. 9.

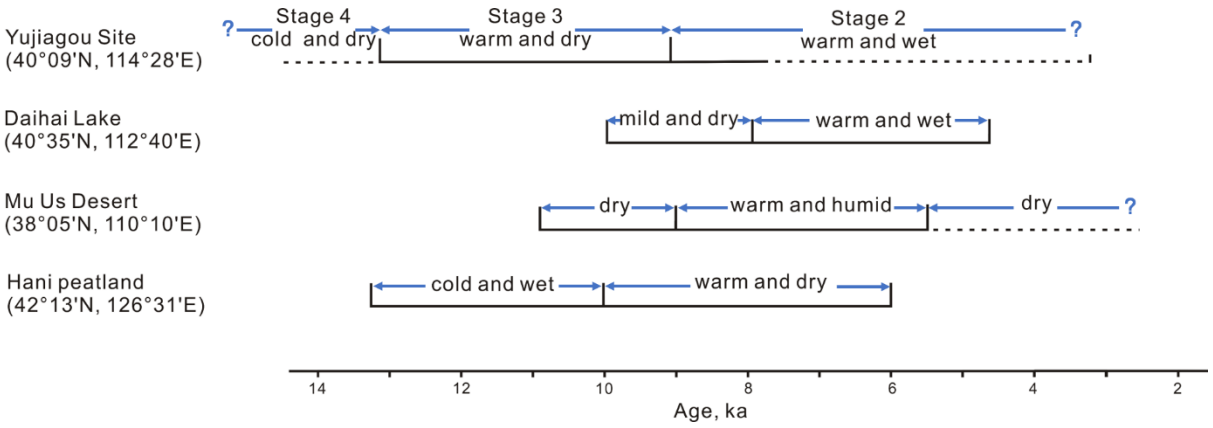
Yujiagou Site
(40°09'N, 114°28'E)
?
Stage 4
cold and dry
Stage 3
warm and dry
Stage 2
warm and wet
?
Daihai Lake
(40°35'N, 112°40'E)
mild and dry
warm and wet
Mu Us Desert
(38°05'N, 110°10'E)
dry
warm and humid
dry
?
Hani peatland
(42°13'N, 126°31'E)
cold and wet
warm and dry
14
12
10
8
6
4
2
Age, ka